www.ietdl.org

Published in IET Communications
Received on 3rd February 2013
Revised on 7th August 2013
Accepted on 16th August 2013
doi: 10.1049/iet-com.2013.0092

ISSN 1751-8628

Robust carrier frequency offset and channel estimation for orthogonal frequency division multiple access downlink systems in the presence of severe adjacent-cell interference

Juinn-Horng Deng, Shu-Min Liao

Communication Research Center and Department of Communication Engineering, Yuan Ze University, Chungli 32003, Taoyuan, Taiwan
E-mail: jh.deng@saturn.yzu.edu.tw

Abstract: This study investigates joint estimation carrier frequency offset (CFO) and channel impulse response (CIR) in the problematic orthogonal frequency division multiple access (OFDMA) downlink scenario at the cell boundary, where a maximum supposition of three adjacent base stations preambles can be received. A novel scheme is proposed for estimating the CFOs and CIRs of different cells. First, the highly efficient joint maximum-likelihood (JML) algorithm is used to enable robust CFO estimation by exploiting the idempotent property of the projection matrix. Next, in order to estimate the precise CIR, the composite CFO-based and circularly shifted preamble signatures are proposed by applying the constrained minimum variance (CMV) algorithm to suppress adjacent-cell interference. Finally, the CFO and CIR estimations are enhanced by an iterative cancellation scheme. To the best of the authors research, there is no publication study proposed joint JML-CFO and CMV-CIR estimators for OFDMA downlink systems with adjacent-cell interference. Simulation results show that the proposed algorithms provide better performance than the conventional estimators and approach the theoretical Cramer–Rao lower bound at the cell boundary over frequency-selective fading channels.

1 Introduction

To achieve high spectrum efficiency and high system capacity, the orthogonal frequency division multiple access (OFDMA) scheme has been applied in many broadband cellular wireless systems, including worldwide interoperability for microwave access (WiMAX) IEEE 802.16e [1] and 3GPP long-term evolution (LTE) [2]. An important function of the OFDMA receiver is to provide robust synchronisation before the data payload is received. With the assistance of a transmitted preamble, the synchronisation process usually includes two major tasks, that is, the estimation of carrier frequency offset (CFO) and channel impulse response (CIR) [3]. Accurate CFO compensation is needed to maintain orthogonality between subcarriers. Without compensation, inter-carrier interference (ICI) can degrade receiver performance. Similarly, accurate channel estimation is also needed for effective equalisation in the frequency domain. In conventional synchronisation algorithms [3–7], CFO and CIR are separately estimated using a simple two-stage approach. Although they enjoy the implementation feasibility, the residual CFO caused by frequency synchronisation errors can substantially degrade CIR estimation performance [8]. Therefore such algorithms are sub-optimal and suffer from the degraded performance as compared with the Cramer–Rao lower bound (CRLB). On the other hand, in the pursuit of the optimal estimation performance, a lot of papers [9–18] in OFDM systems have been proposed by a joint CFO and CIR estimation schemes. In these schemes, CFO and CIR estimations are achieved iteratively in expectation–maximisation [9–12] or by alternating projection algorithms [13, 14]. Besides, studies by Chen *et al.* [15], Morelli and Mengali [16] and Hwang *et al.* [17] have also proposed joint CFO and CIR estimation schemes that achieve performance approaching that of CRLB. However, these estimators were designed for single-cell OFDM systems rather than for OFDMA downlink systems in the presence of severe adjacent-cell interference.

Moreover, since most OFDMA-based cellular systems have frequency reuse factor of one and sector antennas, where each sector of the base station has its own cell-specific preamble sequence. However, at the cell edge, severe interference from three adjacent base stations exists, and therefore hinders the synchronisation techniques in [9–17] to work well. In this case, the users at the cell boundary will suffer from a small signal-to-interference and noise ratio (SINR) performance because of the adjacent-cell and ICI interferences induced by the synchronisation errors. It will increase an outage rate at the cell boundary. Presently, the crucial requirement for achieving high cell-edge throughput is the downlink coordinated

multi-point transmission/reception system [18]. For improved SINR performance and reduced outage rate at the cell boundary, this study developed an optimal synchronisation algorithm for reducing cell-edge interference and for achieving a performance approaching that of the ideal CRLB. First, a joint maximum-likelihood (JML) formulation is used for simultaneous estimation of multiple CFOs and CIRs for three interfering cells. A highly efficient JML algorithm is then derived for accurately estimating CFOs in terms of coarse fast Fourier transform (FFT) peak finding and a refining zoom-FFT. Second, the estimated CFOs are used to construct phase-rotated and circularly shifted preamble sequences for all sectors. The sequences are then applied in the subsequent constrained minimum variance (CMV) algorithm [19, 20] to estimate the CIR for each cell while suppressing interference from the other two cells. Finally, the estimated CFOs and CIRs are used for separate regeneration of the received preamble signals for all cells. Thus, the iterative interference cancellation [21, 22] procedure further improves the CFO/CIR estimation accuracy in each cell. The resultant estimator is referred to as a robust JML-CMV estimator. Furthermore, CRLBs derived for the CFO and CIR estimations are used as benchmarks for comparing the performance of the proposed JML-CMV estimator. The simulation results for the addressed severe adjacent-cell interference scenario confirm that the robustness of the proposed estimator approaches that of the CRLB. To the best of our knowledge, there is no publication paper proposed joint CFO and CIR estimation for OFDMA downlink systems with adjacent-cell interference.

The paper is organised as follows. Section 2 formulates the received signal model with CFO and CIR effects for a cell-edge environment. In Section 3, the JML-CMV estimator structure and the associated algorithms are developed. Section 4 derives the CRLB of CFO and CIR estimation. Section 5 presents the simulation results, including mean square error (MSE) and output preamble SINR, which confirm the excellent performance of the proposed estimator. Finally, conclusions are made in Section 6.

2 System and signal model

A downlink packet-based OFDMA cellular system with three cell reuse architecture is considered in Fig. 1. Users at the cell boundary simultaneously receive cochannel signals from all three sectors of adjacent cells. The severe adjacent-cell interference generated in this scenario causes difficulty for the user when performing synchronisation tasks. Fig. 2 shows the OFDMA transceiver structure, in which the start preamble in each sector downlink frame is used for CFO and CIR estimations. In WiMAX, the adjacent cells are synchronised to the same frame timing, and employ the preambles with mutually orthogonal subcarrier sets which are interleaved and offset by $i = 0, 1, 2$ subcarriers. The transmitted N-point preamble symbol vector $\boldsymbol{s}^{(i)} = [s^{(i)}(0) \cdots s^{(i)}(N-1)]^{\mathrm{T}}$ of the ith cell can then be expressed as

$$\boldsymbol{s}^{(i)} = \boldsymbol{F}^{\mathrm{H}} \boldsymbol{d}^{(i)} \tag{1}$$

where $\boldsymbol{F}^{\mathrm{H}}$ denotes the $N \times N$ orthonormal inverse fast Fourier transform (IFFT) matrix and $\boldsymbol{d}^{(i)} = [d^{(i)}(0) \cdots d^{(i)}(N-1)]^{\mathrm{T}}$ is

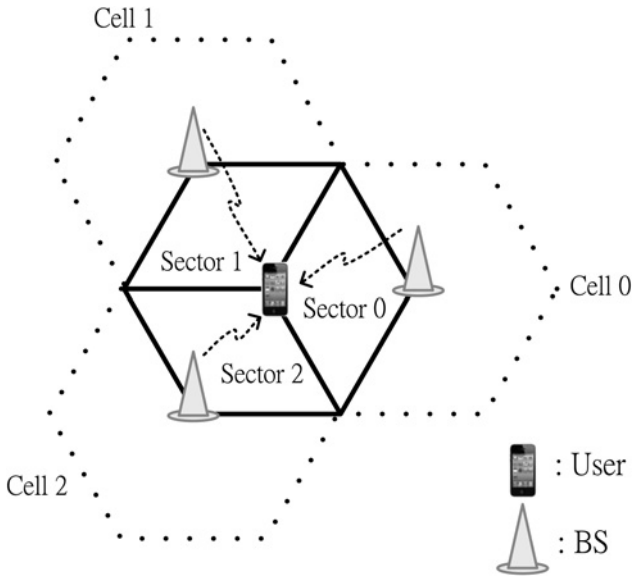

Fig. 1 *OFDMA cellular system with three cell reuse architecture*

the frequency-domain training sequence in which

$$d^{(i)}(n) = \begin{cases} u^{(i)}\left(\dfrac{n-i-1}{3}\right), & n = 3k + i + 1, \\ & k = 0, 1, \ldots, M \\ 0, & \text{otherwise} \end{cases} \tag{2}$$

where $u^{(i)}(k)$ is the specific frequency-domain Zadoff–Chu sequence code [23] with the number of length $M = \text{int}(N/3)$ for the ith cell, $i = 0, 1, 2$. The int(x) means the largest integer not exceeding x. An N_g-point cyclic prefix (CP) is then inserted to avoid the inter-symbol interference caused by the multipath channel. Let $\boldsymbol{h}^{(i)} = [h^{(i)}(0) \cdots h^{(i)}(L-1)]^{\mathrm{T}}$ denote the unknown discrete-time CIR between the user and the ith base station, where channel length $L < N_g$. Similarly, let $f_{\Delta}^{(i)}$ denote the unknown CFO with normalisation of subcarrier spacing for the ith base station. Besides the CFOs, there are carrier phase offsets (CPOs) too. Owing to the constant phase property existing in different subcarriers in [17], the CPOs can be accommodated into the corresponding CIRs. In Fig. 2*b*, we assume that the user is located at the cell boundary, where it receives the superimposed preambles from the three adjacent cells with different CIRs and CFOs. With adjacent-cell interference, the equivalent received signal vector $\boldsymbol{y} = [y_0 \cdots y_{N-1}]^{\mathrm{T}}$ after CP removal can be written as

$$\boldsymbol{y} = \sum_{i=0}^{2} \boldsymbol{G}(f_{\Delta}^{(i)}) \boldsymbol{S}^{(i)} \boldsymbol{h}^{(i)} + \boldsymbol{w} \tag{3}$$

where $\boldsymbol{w} = [w_0 \cdots w_{N-1}]^{\mathrm{T}}$ denotes the $N \times 1$ complex white Gaussian noise with zero mean and covariance matrix $\sigma_w^2 \boldsymbol{I}_{N \times N}$. The $\boldsymbol{G}(f_{\Delta}^{(i)}) = \text{diag}\{1, \mathrm{e}^{\mathrm{j}2\pi f_{\Delta}^{(i)}/N}, \ldots, \mathrm{e}^{\mathrm{j}2\pi f_{\Delta}^{(i)}(N-1)/N}\}$ denotes the $N \times N$ diagonal matrix because of CFO of the ith cell. The $\boldsymbol{S}^{(i)} = [\boldsymbol{s}_0^{(i)} \cdots \boldsymbol{s}_{L-1}^{(i)}]$ is the $N \times L$ circulant matrix, in which the kth column $\boldsymbol{s}_k^{(i)}$ is the rotated preamble vector after k cyclic shifts of the base code $\boldsymbol{s}_0^{(i)}$. Next, based on the IFFT of the frequency-domain preamble code in (1) and (2), the time-domain N-point polyphase Zadoff–Chu sequence can be denoted as the base code $\boldsymbol{s}_0^{(i)} = \boldsymbol{F}^{\mathrm{H}} \boldsymbol{d}^{(i)}$ with

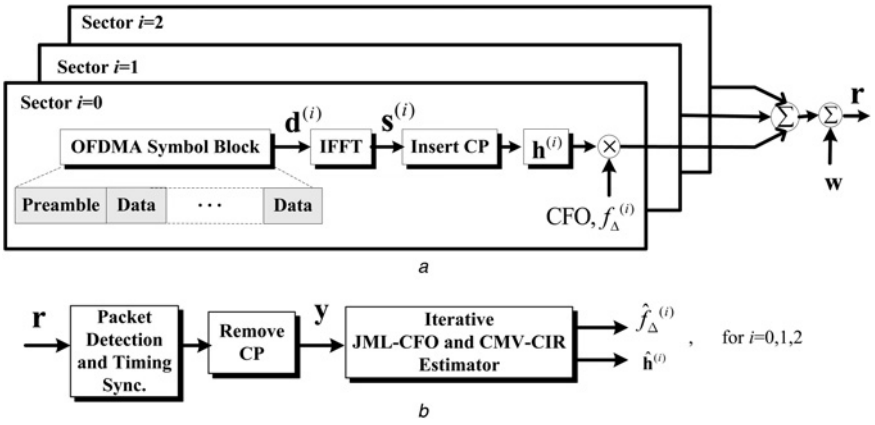

Fig. 2 *Block diagram of the OFDMA downlink transceiver system*

a Transmitter
b Receiver

$u^{(i)}(k) = \frac{1}{\sqrt{M}} \exp\left(\mathrm{j}\pi k^2 (i+1)/M\right)$, where i and M are relatively prime. Then, the time-domain Zadoff–Chu sequence has well autocorrelation and cross-correlation properties, that is, $\langle \boldsymbol{s}_k^{(i)}, \boldsymbol{s}_m^{(i)} \rangle = 1$ for $k = m$ and $\langle \boldsymbol{s}_k^{(i)}, \boldsymbol{s}_m^{(i)} \rangle \simeq 0$ for $k \neq m$.

In the presence of severe adjacent-cell interference, we attempt to estimate the parameter set $\{f_\Delta^{(i)}, \boldsymbol{h}^{(i)}\}_{i=0}^{2}$ in the received signal model (3) and to cancel the adjacent-cell interference so that the user can properly link to the base station. Next, the popular CFO estimators, that is, cross-correlation-based method, are readily found in the literatures [24, 25]. For example, the maximum-likelihood estimator (MLE) [24], which is the optimum estimator under additive white Gaussian noise (AWGN), is used in the post-despread signal of two contiguous preambles to estimate the CFO of the ith cell, that is

$$\hat{f}_\Delta^{(i)} = \frac{1}{2\pi} \tan^{-1} \left\{ \frac{\sum_{l=0}^{L-1} \mathrm{Im}\left[\left(\mathrm{diag}\left(\boldsymbol{s}_l^{(i)\mathrm{H}}\right)\boldsymbol{y}(k+1)\right)^{\mathrm{H}} \left(\mathrm{diag}\left(\boldsymbol{s}_l^{(i)\mathrm{H}}\right)\boldsymbol{y}(k)\right)\right]}{\sum_{l=0}^{L-1} \mathrm{Re}\left[\left(\mathrm{diag}\left(\boldsymbol{s}_l^{(i)\mathrm{H}}\right)\boldsymbol{y}(k+1)\right)^{\mathrm{H}} \left(\mathrm{diag}\left(\boldsymbol{s}_l^{(i)\mathrm{H}}\right)\boldsymbol{y}(k)\right)\right]} \right\} \tag{4}$$

where $\boldsymbol{s}_l^{(i)\mathrm{H}}\boldsymbol{y}(k)$ is the despreaded signal of the lth path of the kth preamble for ith cell. The MLE algorithm in (4) is used as the benchmark method to be compared with the proposed algorithm, which will be simulated in Section 5. Most existing frequency offset estimators are developed based on the assumption of no or little interference (i.e. AWGN). In the presence of strong interference, these estimators often degrade seriously. Therefore interference cancellation must be performed before frequency offset estimation.

3 Efficient multi-CFO/CIR estimation by iterative JML-CMV method

Since the received signal in (3) involves the multi-CFO/CIR and adjacent-cell interference, the orthogonality between preambles is destroyed by the difference in CFOs and mutual interference. This section therefore describes how the proposed iterative JML-CMV method with interference cancellation is used to estimate ith cell parameters $\{f_\Delta^{(i)}, \boldsymbol{h}^{(i)}\}$. Fig. 3 shows an overall schematic diagram of the proposed method. The iterative estimator includes the JML-CFO estimator, CMV-CIR estimator, signal reconstruction and the selected adjacent-cell interference combiner. The design of the iterative estimator involves the following procedures. First, the multi-cell JML-CFO estimator performs a CFO estimation. Second, the multipath channel response of multi-cell is estimated by exploiting the estimated frequency offset and CMV estimator. Next, the multi-cell signal reconstruction is done by exploiting the carrier frequency estimate, path gain estimate and the known preamble sequence. Finally, the reconstructed multi-cell signal waveforms are selectively combined and subtracted from the received data sent to the next iteration to obtain the more accurate multi-cell CFO and CIR parameters.

3.1 JML algorithm for CFO estimation

According to (3), the likelihood function of $\left\{f_\Delta^{(i)}, \boldsymbol{h}^{(i)}\right\}$ with $i = 0, 1, 2$ for the received data vector $\boldsymbol{y}$ can be written as

$$\begin{aligned} & p\left(\boldsymbol{y}; \{f_\Delta^{(i)}, \boldsymbol{h}^{(i)}, i = 0, 1, 2\}\right) \\ &= \frac{1}{\left(\pi\sigma^2\right)^N} \exp\left\{ -\frac{1}{\sigma^2} \left\| \boldsymbol{y} - \sum_{i=0}^{2} \boldsymbol{G}(f_\Delta^{(i)}) \boldsymbol{S}^{(i)} \boldsymbol{h}^{(i)} \right\|^2 \right\} \\ &= \frac{1}{\left(\pi\sigma^2\right)^N} \exp\left\{ -\frac{1}{\sigma^2} \left\| \boldsymbol{y} - \bar{\boldsymbol{G}}(\boldsymbol{f}_\Delta) \bar{\boldsymbol{S}} \bar{\boldsymbol{h}} \right\|^2 \right\} \end{aligned} \tag{5}$$

where $\boldsymbol{f}_\Delta = \left[f_\Delta^{(0)} f_\Delta^{(1)} f_\Delta^{(2)}\right]^{\mathrm{T}}$ is a 3×1 vector. The composite preamble matrix is $\bar{\boldsymbol{S}} = \mathrm{diag}\left(\boldsymbol{S}^{(0)}, \boldsymbol{S}^{(1)}, \boldsymbol{S}^{(2)}\right)$ with dimensions of $3N \times 3L$, the CIR is $\bar{\boldsymbol{h}} = [\boldsymbol{h}^{(0)\mathrm{T}} \boldsymbol{h}^{(1)\mathrm{T}} \boldsymbol{h}^{(2)\mathrm{T}}]^{\mathrm{T}}$ with dimensions of $3L \times 1$, and the CFO is $\bar{\boldsymbol{G}}(\boldsymbol{f}_\Delta) = \left[\boldsymbol{G}(f_\Delta^{(0)}) \boldsymbol{G}(f_\Delta^{(1)}) \boldsymbol{G}(f_\Delta^{(2)})\right]$ with dimensions of $N \times 3N$. Note that the function of the MLE is equivalent to minimising the following metric

$$\hat{\boldsymbol{D}} = \left\{\hat{\boldsymbol{f}}_\Delta, \hat{\bar{\boldsymbol{h}}}\right\} = \arg \min_{\{\boldsymbol{f}_\Delta, \bar{\boldsymbol{h}}\}} \left\| \boldsymbol{y} - \bar{\boldsymbol{G}}(\boldsymbol{f}_\Delta) \bar{\boldsymbol{S}} \bar{\boldsymbol{h}} \right\|^2 \tag{6}$$

doi: 10.1049/iet-com.2013.0092

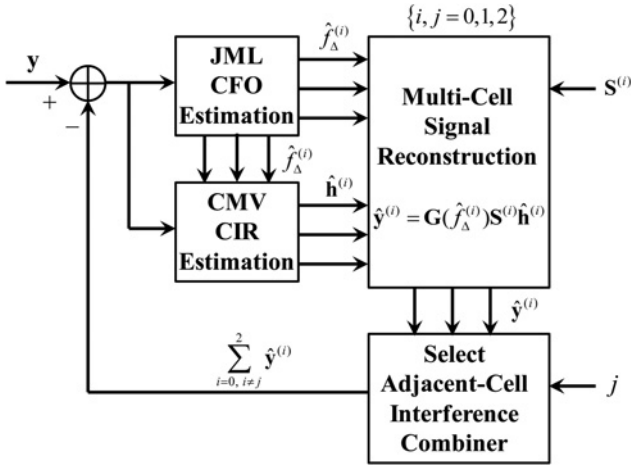

Fig. 3 *Block diagram of the iterative JML-CFO and CMV-CIR estimation algorithm*

If the estimated CFO $\hat{f}_\Delta$ is known, the composite channel estimate $\hat{\bar{h}}$ with $3L \times 1$ dimension is easily obtained by finding the linear least-square (LS) solution

$$\hat{\bar{h}} = \left(\bar{S}^{\mathrm{H}}\bar{S}\right)^{-1}\bar{S}^{\mathrm{H}}\bar{G}^{\mathrm{H}}(\hat{f}_\Delta)y \tag{7}$$

The $\hat{\bar{h}}$ is substituted into (6), and after some derivation, the metric for CFO estimation can be rewritten as

$$\begin{aligned}\hat{D} &= \arg\min_{\{f_\Delta\}}\left\|\bar{G}^{\mathrm{H}}(f_\Delta)y - \bar{S}\hat{\bar{h}}\right\|^2 \\ &= \arg\max_{\{f_\Delta\}}\left\|P_{\bar{S}}\bar{y}(f_\Delta)\right\|^2\end{aligned} \tag{8}$$

where $\bar{y}(f_\Delta) = \bar{G}^{\mathrm{H}}(f_\Delta)y$ denotes the $3N \times 1$ received signal vector with CFO effect, and $P_{\bar{S}} = \bar{S}\left(\bar{S}^{\mathrm{H}}\bar{S}\right)^{-1}\bar{S}^{\mathrm{H}}$ is the $3N \times 3N$ pre-computed projection matrix onto the column span of $\bar{S}$. According to (8), the computational expense of a brute-force grid search for the JML-CFO is too high. Therefore an efficient JML-CFO estimation scheme is proposed.

Since $P_{\bar{S}}$ is known and idempotent, the JML-CFO estimation is equivalent to maximising

$$\hat{f}_\Delta = \arg\max_{\{f_\Delta\}}\left\{y^{\mathrm{H}}\Psi(f_\Delta)P_{\bar{S}}\Psi^{\mathrm{H}}(f_\Delta)y\right\} \tag{9}$$

where the $N \times 3N$ matrix of CFO effect is denoted by $\Psi(f_\Delta) = [\Psi(f_\Delta^{(0)})\Psi(f_\Delta^{(1)})\Psi(f_\Delta^{(2)})]$ with the $N \times N$ diagonal matrix of $\Psi(f_\Delta^{(i)}) = \mathrm{diag}\{1, \mathrm{e}^{\mathrm{j}2\pi f_\Delta^{(i)}/N}, \ldots, \mathrm{e}^{\mathrm{j}2\pi f_\Delta^{(i)}(N-1)/N}\}$ for $i = 0, 1, 2$. The efficient algorithm is obtained by rewriting (9) as

$$\hat{f}_\Delta = \arg\max_{\{f_\Delta\}}\left\{e^{\mathrm{H}}(f_\Delta)\left(P_{\bar{S}} \odot (\bar{y}^*\bar{y}^{\mathrm{T}})\right)e(f_\Delta)\right\} \tag{10}$$

where the $3N \times 1$ received signal vector is $\bar{y} = [y^{\mathrm{T}}y^{\mathrm{T}}y^{\mathrm{T}}]^{\mathrm{T}}$, the $3N \times 1$ composite CFO vector is $e(f_\Delta) = [e(f_\Delta^{(0)})^{\mathrm{T}}e(f_\Delta^{(1)})^{\mathrm{T}}e(f_\Delta^{(2)})^{\mathrm{T}}]^{\mathrm{T}}$ with the $N \times 1$vector of $e(f_\Delta^{(i)}) = [1, \mathrm{e}^{-\mathrm{j}2\pi f_\Delta^{(i)}/N}, \ldots, \mathrm{e}^{-\mathrm{j}2\pi f_\Delta^{(i)}(N-1)/N}]^{\mathrm{T}}$ and $\odot$ denotes an element-wise multiplication operation. Clearly, the $3N \times 3N$ matrix $A = P_{\bar{S}} \odot (\bar{y}^*\bar{y}^{\mathrm{T}})$ is easily obtained by element-wise multiplication of the known matrix $P_{\bar{S}}$ with the vector product of the received signal vector $\bar{y}$. Since A is a conjugate symmetric matrix, the scalar of $e^{\mathrm{H}}(f_\Delta)Ae(f_\Delta)$ in (10) can be derived as a polynomial function of $\mathrm{e}^{-\mathrm{j}2\pi k f_\Delta^{(i)}/N}$. That is, $a_k^{(i)}$ is used to denote the summation of the kth subdiagonal elements of the ith submatrix $A^{(i)} = A[iN+1:(i+1)N, iN+1:(i+1)N]$ with $i = 0, 1, 2$, that is

$$\bar{a}_k^{(i)} = \sum_{n=1}^{N} a_{\tilde{n}_k, n}^{(i)} \tag{11}$$

where $\tilde{n}_k = \mathrm{mod}(n + k - 1, N) + 1$ is denoted by the modulo operation and $a_{\tilde{n}_k, n}^{(i)}$ is the $(\tilde{n}_k, n)$th element of the ith submatrix $A^{(i)}$. Note that because $P_{\bar{S}}$ involves the submatrix diagonal property because of $\bar{S}$, the matrix A can be expressed by $A = \mathrm{diag}\{A^{(0)}, A^{(1)}, A^{(2)}\}$. Therefore, substituting A and $\bar{a}_k^{(i)}$ into (10), it can be derived by

$$\begin{aligned}\hat{f}_\Delta &= \arg\max_{\{f_\Delta\}}\left\{\left[e\left(f_\Delta^{(0)}\right)^{\mathrm{H}}e\left(f_\Delta^{(1)}\right)^{\mathrm{H}}e\left(f_\Delta^{(2)}\right)^{\mathrm{H}}\right]\right. \\ &\quad \left.\times\begin{bmatrix}A^{(0)} & 0 & 0\\ 0 & A^{(1)} & 0\\ 0 & 0 & A^{(2)}\end{bmatrix}\begin{bmatrix}e(f_\Delta^{(0)})\\ e(f_\Delta^{(1)})\\ e(f_\Delta^{(2)})\end{bmatrix}\right\} \\ &= e^{\mathrm{H}}\left(f_\Delta^{(0)}\right)A^{(0)}e\left(f_\Delta^{(0)}\right) + e^{\mathrm{H}}\left(f_\Delta^{(1)}\right)A^{(1)}e\left(f_\Delta^{(1)}\right) \\ &\quad + e^{\mathrm{H}}\left(f_\Delta^{(2)}\right)A^{(2)}e\left(f_\Delta^{(2)}\right) \\ &= \sum_{i=0}^{2}\left\{\bar{a}_0^{(i)} + 2\mathrm{Re}\left\{\sum_{k=1}^{N-1}\bar{a}_0^{(i)}\mathrm{e}^{-\mathrm{j}2\pi k f_\Delta^{(i)}/N}\right\}\right\}\end{aligned} \tag{12}$$

where $\mathrm{Re}(\cdot)$ denotes the real part of a complex number. The above skill is called polynomial approach. Thus, the problem in (12) can be solved in terms of an FFT peak finding. However, a large FFT size is needed for an accurate estimate of CFO. The frequency bin resolution problem is solved by first applying a coarse FFT to approximate the peak locations and then applying the Zoom-FFT algorithm [26] to refine the peak locations. The efficiency of this procedure substantially reduces the computational burden. The overall JML-CFO algorithm is summarised in Fig. 4*a*.

3.2 CMV algorithm for channel estimation

After the JML-CFO process is used to obtain the multi-CFO estimate $\hat{f}_\Delta$, the frequency-offset and circularly shifted preamble vector $\tilde{s}_l^{(i)}$ with $N \times 1$ dimension is obtained as follows

$$\begin{aligned}\tilde{s}_l^{(i)} &= G\left(\hat{f}_\Delta^{(i)}\right)s_l^{(i)}, \quad i = 0,\ 1,\ 2, \\ &\quad l = 0,\ 1,\ \ldots,\ L-1\end{aligned} \tag{13}$$

Next, if the JML-CFO method provides an accurate multi-CFO estimate $\hat{f}_\Delta$, the composite preamble vector in

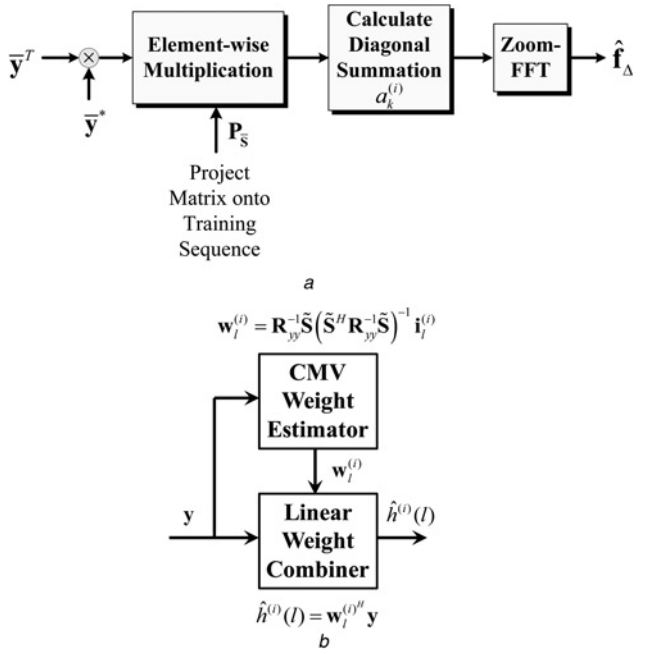

Fig. 4 *Block diagram of JML-CFO and CMV-CIR algorithm*
a JML-CFO
b CMV-CIR

(13) can be used to approach the received signal in (3), that is

$$\boldsymbol{y} \simeq \sum_{i=0}^{2} \tilde{\boldsymbol{S}}^{(i)} \boldsymbol{h}^{(i)} + \boldsymbol{w} \tag{14}$$

where $\tilde{\boldsymbol{S}}^{(i)} = [\tilde{\boldsymbol{s}}_0^{(i)} \cdots \tilde{\boldsymbol{s}}_{L-1}^{(i)}]$ is the frequency-offset and circularly shifted preamble matrix with dimensions of $N \times L$. In (14), $\tilde{\boldsymbol{s}}_l^{(i)}$ is treated as the known response vector associated with the unknown CIR tap $\hat{h}^{(i)}(l)$ and is used in the following interference suppression scheme for individually estimating all CIR taps. In doing so, we use a linear combiner to suppress the adjacent-cell and inter-tap interferences. The overall JML-CMV algorithm is summarised in Fig. 4*b*, that is

$$\hat{h}^{(i)}(l) = \boldsymbol{w}_l^{(i)\mathrm{H}} \boldsymbol{y} \tag{15}$$

where $\boldsymbol{w}_l^{(i)}$ is the $N \times 1$ weight vector for estimating the lth CIR tap of the ith cell. The weight vector can be designed according to the CMV criterion, which minimises the combiner output power while maintaining a unity response needed for the desired tap. That is, the CMV criterion can determine the weight vector as follows

$$\begin{aligned} &\min_{\boldsymbol{w}_l^{(i)}} \boldsymbol{w}_l^{(i)\mathrm{H}} \boldsymbol{R}_{yy} \boldsymbol{w}_l^{(i)} \\ &\text{subjectto: } \boldsymbol{w}_l^{(i)\mathrm{H}} \tilde{\boldsymbol{s}}_l^{(j)} = 1, \quad i = j \\ &\boldsymbol{w}_l^{(i)\mathrm{H}} \tilde{\boldsymbol{s}}_l^{(j)} = 0, \quad i \neq j \\ &\boldsymbol{w}_l^{(i)\mathrm{H}} \tilde{\boldsymbol{s}}_m^{(j)} = 0, \quad l \neq m \end{aligned} \tag{16}$$

for $l,\ m = 0,\ 1,\ \ldots,\ L-1$, and $i, j = 0,\ 1,\ 2$, where

$$\begin{aligned} \boldsymbol{R}_{yy} &= E\left(\boldsymbol{y}(i)\boldsymbol{y}^{\mathrm{H}}(i)\right) \\ &= \sum_{i=0}^{2} \sum_{l=0}^{L-1} \sigma_l^{(i)^2} \tilde{\boldsymbol{s}}_l^{(i)} \tilde{\boldsymbol{s}}_l^{(i)\mathrm{H}} + \sigma_w^2 \boldsymbol{I} \end{aligned} \tag{17}$$

with $\sigma_l^{(i)^2} = E\left(h^{(i)}(l) h^{(i)*}(l)\right)$. The solution of the CMV weight vector in (16) can be determined by the Lagrange multiply constraint, that is

$$\begin{aligned} &\nabla_{\boldsymbol{w}_l^{(i)}} \left\{ \boldsymbol{w}_l^{(i)\mathrm{H}} \boldsymbol{R}_{yy} \boldsymbol{w}_l^{(i)} \right\} \\ &\quad - \sum_{j=0}^{2} \sum_{m=0}^{L-1} \lambda_m^{(j)} \nabla_{\boldsymbol{w}_l^{(i)}} \left\{ \boldsymbol{w}_l^{(i)\mathrm{H}} \tilde{\boldsymbol{s}}_m^{(j)} - \delta[i-j]\delta[l-m] \right\} = 0 \\ &\boldsymbol{w}_l^{(i)\mathrm{H}} \tilde{\boldsymbol{s}}_m^{(j)} = \delta[i-j]\delta[l-m] \end{aligned} \tag{18}$$

where $\nabla_{\boldsymbol{w}_l^{(i)}}\{\cdot\}$ is defined by the complex gradient of $\{\cdot\}$ with respect to $\boldsymbol{w}_l^{(i)}$, $\delta[\cdot]$ is the delta function and $\lambda_m^{(j)}$ is the multiply constraint. Based on the gradient of (16), it can be calculated by

$$\boldsymbol{R}_{yy} \boldsymbol{w}_l^{(i)} = \tilde{\boldsymbol{S}} \boldsymbol{\lambda} \tag{19}$$

$$\boldsymbol{w}_l^{(i)\mathrm{H}} \tilde{\boldsymbol{S}} = \boldsymbol{i}_l^{(i)^{\mathrm{T}}} \tag{20}$$

where $\tilde{\boldsymbol{S}} = [\tilde{\boldsymbol{S}}^{(0)} \tilde{\boldsymbol{S}}^{(1)} \tilde{\boldsymbol{S}}^{(2)}]$ is the composite frequency-offset preamble matrix with dimensions of $N \times 3L$, $\boldsymbol{\lambda} = [\lambda_0^{(0)},\ \lambda_1^{(0)},\ \ldots,\ \lambda_{L-1}^{(0)},\ \lambda_0^{(1)},\ \ldots,\ \lambda_{L-1}^{(2)}]^{\mathrm{T}}$ is the composite multiply constraint vector with dimensions of $3L \times 1$, and $\boldsymbol{i}_l^{(i)}$ is the $(iL + l)$th column of the identity matrix $\boldsymbol{I}_{3L \times 3L}$. Next, substituting the weight vector in (19), that is, $\boldsymbol{w}_l^{(i)} = \boldsymbol{R}_{yy}^{-1} \tilde{\boldsymbol{S}} \boldsymbol{\lambda}$, into (20), the composite multiply constraint can be obtained by

$$\boldsymbol{\lambda} = \left(\tilde{\boldsymbol{S}}^{\mathrm{H}} \boldsymbol{R}_{yy}^{-1} \tilde{\boldsymbol{S}} \right)^{-1} \boldsymbol{i}_l^{(i)} \tag{21}$$

Moreover, by substituting (21) into (19), the CMV weight vector can be expressed as

$$\boldsymbol{w}_l^{(i)} = \boldsymbol{R}_{yy}^{-1} \tilde{\boldsymbol{S}} \left(\tilde{\boldsymbol{S}}^{\mathrm{H}} \boldsymbol{R}_{yy}^{-1} \tilde{\boldsymbol{S}} \right)^{-1} \boldsymbol{i}_l^{(i)} \tag{22}$$

Notably, by applying the CMV weight vector as reported in (22), all CIR taps can be estimated by applying the proposed procedure (15). Therefore the overall CIR estimates can be collected and formed by

$$\hat{\boldsymbol{h}}^{(i)} = [\hat{h}^{(i)}(0) \hat{h}^{(i)}(1) \cdots \hat{h}^{(i)}(L-1)]^{\mathrm{T}}, \quad i = 0,\ 1,\ 2 \tag{23}$$

3.3 Iterative interference cancellation

Next, the iterative interference cancellation scheme for improving the accuracy of the estimator is described. First, with $\hat{h}^{(i)}$ and $\hat{f}_{\Delta}^{(i)}$ available in Sections 3.1 and 3.2, the preamble signal received from the ith cell transmission is then reconstructed as

$$\hat{\boldsymbol{y}}^{(i)} = \boldsymbol{G}\left(\hat{f}_{\Delta}^{(i)}\right) \boldsymbol{S}^{(i)} \hat{\boldsymbol{h}}^{(i)} \tag{24}$$

doi: 10.1049/iet-com.2013.0092

Table 1 Algorithm summary of iterative receiver

1.	compute $\hat{\boldsymbol{f}}_{\Delta}$ according to (12)
2.	compute $\hat{\boldsymbol{h}}^{(i)}$, $i=0, 1, 2$, according to (15), (22) and (23)
3.	obtain $\hat{\boldsymbol{y}}^{(i)}$ and $\tilde{\boldsymbol{y}}^{(j)}$ according to (24) and (25), respectively
4.	check convergence of $\Delta \boldsymbol{h}k$ in Section3.3. If yes, go to 5. If not, set $k=k+1$ and go to 1 with replacing $\boldsymbol{y}$ by $\tilde{\boldsymbol{y}}^{(j)}$
5.	finally obtain the estimated CFO $\hat{\boldsymbol{f}}_{\Delta}$ and CIR $\hat{\boldsymbol{h}}^{(i)}$, $i=0, 1, 2$

for $i=0, 1, 2$. Then, the reconstructed preamble signals are subtracted from the received signal sent to the next iteration. This leads to the residual signal of the jth cell reception given by

$$\tilde{\boldsymbol{y}}^{(j)} = \boldsymbol{y} - \sum_{\substack{i=0 \\ i\neq j}}^{2} \hat{\boldsymbol{y}}^{(i)} \tag{25}$$

Using $\tilde{\boldsymbol{y}}^{(j)}$ as the new input of the JML and CMV estimators effectively improves the poor convergence of CFO and CIR estimation of the jth cell for $j=0, 1, 2$. Next, about the stop criterion for iteration, the converged CIR error can be used to check the following criterion: $\Delta \boldsymbol{h}_k = \frac{1}{3}\sum_{i=0}^{2} \left\| \hat{\boldsymbol{h}}_k^{(i)} - \hat{\boldsymbol{h}}_{k-1}^{(i)} \right\| \Big/ \left\| \hat{\boldsymbol{h}}_{k-1}^{(i)} \right\| < \varepsilon$, where k denotes the iteration number and ε is the percentage of the estimated CIR difference, for example, $\varepsilon = 1\%$. Finally, based on the algorithms proposed in Section 3, the iterative JML and CMV estimators can be summarised in Table 1 for detailed description. Section 5 describes the results of computer simulations used to confirm the performance of the iterative JML-CMV algorithm. To provide a reference for performance comparison, the CRLB is derived in the next section.

4 Computational complexity and performance analysis

In Section 3, the multi-CFO/CIR estimator is proposed for the downlink OFDMA system. According to the previous three subsection algorithms, we will calculate the computational complexity and compare with the conventional methods. Next, the CRLB performances of both CFO and CIR estimations are analysed in this section.

4.1 Complexity analysis

This subsection analyses and compares the computational complexity of the proposed iterative JML-CMV method with conventional estimator in [17] and the cross-correlation-based CFO estimator in (4). In general, the trade-off between system performance and computational complexity is an issue depending on the degree of freedom, for example, the length of preamble sequence N. A larger preamble sequence size will provide better interference suppression, but lead to high computational complexity. For our proposed algorithm, the major computation is the matrix inversion and multiplication of $\boldsymbol{R}_{yy}^{-1}\tilde{\boldsymbol{S}}$ in (22) of Section 3.2, which involves the computational complexity (in number of complexity multiplications) being about $O(N^3+3N^2L)$. Besides, for the computational load of Sections 3.1 and 3.3, that is, CFO estimator in (12) and interference cancellation in (24), the complexities of the two algorithms are computed as $O(9N^2)$ and $O(3N^2+NL)$, respectively. The overall complexity of each iteration is about $O(N^3+3N^2L+12N^2+NL)$ for the proposed JML-CMV algorithms. Note that the computational load is approximately $O(N^3)$ because of N being larger than the multipath size L. With the preamble sequence size N being shortened, the computational loading will be greatly reduced. For comparison, the approximate complexity of the JML method in [17] with the least-square estimator and CFO searcher is about $O(N^2)$. Next, the complexity of the cross-correlation-based CFO estimator in (4) is about $O(18NL)$ because of the correlation of the preamble sequence. Although the proposed estimator requires higher computational complexity compared with the conventional estimators. However, in next section, the simulation results will confirm that the proposed method outperforms the conventional estimators. Especially, the proposed method with the shortened preamble size can still provide the robust performance, which utilises the moderate computational complexity.

4.2 Performance analysis

In this section, the CRLBs of both the CFO and the CIR estimations of the OFDMA system are derived for the performance benchmark of the proposed scheme. That is, for the ideal scenario, the interferences of other cells can be perfectly cancelled and the received signal of the desired single cell is used to estimate CFO and CIR parameters. First, the likelihood function of the parameter set $\boldsymbol{\theta} = \{f_{\Delta}, \boldsymbol{h}\}$ of the desired single cell is used to rewrite the received data vector and the log-likelihood function as

$$\boldsymbol{y} = \boldsymbol{G}(f_{\Delta})\boldsymbol{S}\boldsymbol{h} + \boldsymbol{w} \tag{26}$$

$$\begin{aligned}\Gamma(\boldsymbol{y}; f_{\Delta}, \boldsymbol{h}) = &-\frac{1}{\sigma^2}(\boldsymbol{y}^{\mathrm{H}} - \boldsymbol{h}^{\mathrm{H}}\boldsymbol{S}^{\mathrm{H}}\boldsymbol{G}^{\mathrm{H}}(f_{\Delta})) \\ &\times (\boldsymbol{y} - \boldsymbol{G}(f_{\Delta})\boldsymbol{S}\boldsymbol{h})\end{aligned} \tag{27}$$

The joint estimation formula can then be applied to express the corresponding CRLB [27] based on the Fisher information matrix $\boldsymbol{J}(\boldsymbol{\theta})$ of the above parameter set $\boldsymbol{\theta}$ as

$$\boldsymbol{J}(\boldsymbol{\theta}) = \begin{bmatrix} -E\left\{\frac{\partial^2 \Gamma(\boldsymbol{y};\ \boldsymbol{\theta})}{\partial^2 f_{\Delta}}\right\} & -E\left\{\frac{\partial^2 \Gamma(\boldsymbol{y};\ \boldsymbol{\theta})}{\partial f_{\Delta}\partial \boldsymbol{h}^{\mathrm{H}}}\right\} \\ -E\left\{\frac{\partial^2 \Gamma(\boldsymbol{y};\ \boldsymbol{\theta})}{\partial \boldsymbol{h}\partial f_{\Delta}}\right\} & -E\left\{\frac{\partial^2 \Gamma(\boldsymbol{y};\ \boldsymbol{\theta})}{\partial \boldsymbol{h}\partial \boldsymbol{h}^{\mathrm{H}}}\right\} \end{bmatrix} \tag{28}$$

Next, the details of the procedure for deriving the four elements as described in (28) are given. To obtain the first and second elements in (28), the first step is deriving $\partial \boldsymbol{G}(f_{\Delta})/\partial f_{\Delta}$

$$\frac{\partial \boldsymbol{G}(f_{\Delta})}{\partial f_{\Delta}} = (\mathrm{j}2\pi)\boldsymbol{N}\boldsymbol{G}(f_{\Delta}) \tag{29}$$

where $\boldsymbol{N}$ is a diagonal matrix, that is, $\boldsymbol{N} = \mathrm{diag}\{1, 1/N, \ldots, (N-1)/N\}$. By exploiting (29), the log-likelihood function

differentiated by f_Δ can be obtained by

$$\frac{\partial \Gamma(\boldsymbol{y};\ \boldsymbol{\theta})}{\partial f_\Delta} = \frac{1}{\sigma^2}\left\{(\mathrm{j}2\pi)\boldsymbol{y}^{\mathrm{H}}\boldsymbol{N}\boldsymbol{G}\left(f_\Delta\right)\boldsymbol{S}\boldsymbol{h} + (-\mathrm{j}2\pi)\boldsymbol{h}^{\mathrm{H}}\boldsymbol{S}^{\mathrm{H}}\boldsymbol{N}\boldsymbol{G}^{\mathrm{H}}\left(f_\Delta\right)\boldsymbol{y}\right\} \tag{30}$$

After differentiating (30) with respect to f_Δ, calculating the average obtains the first element of (28)

$$\begin{aligned} -E\left\{\frac{\partial^2 \Gamma(\boldsymbol{y};\ \boldsymbol{\theta})}{\partial f_\Delta^2}\right\} &= \frac{1}{\sigma^2}E\left\{8\pi^2\boldsymbol{y}^{\mathrm{H}}\boldsymbol{N}^2\boldsymbol{G}(f_\Delta)\boldsymbol{S}\boldsymbol{h}\right\} \\ &= \frac{1}{\sigma^2}8\pi^2 E\left\{\boldsymbol{h}^{\mathrm{H}}\boldsymbol{S}^{\mathrm{H}}\boldsymbol{G}^{\mathrm{H}}(f_\Delta) + \boldsymbol{n}^{\mathrm{H}}\right\} \\ &\quad \times \boldsymbol{N}^2\mathbf{G}(f_\Delta)\boldsymbol{S}\boldsymbol{h} \\ &= \frac{1}{\sigma^2}8\pi^2\boldsymbol{h}^{\mathrm{H}}\boldsymbol{S}^{\mathrm{H}}\boldsymbol{N}^2\boldsymbol{S}\boldsymbol{h} \end{aligned} \tag{31}$$

where $\boldsymbol{y}$ is the received data vector in (26) and the noise vector is zero mean $E(\boldsymbol{n}^{\mathrm{H}}) = \mathbf{0}$. Differentiating (30) with respect to $\boldsymbol{h}$ and calculating the average then gives the second element of (28)

$$\begin{aligned} -E\left\{\frac{\partial^2 \Gamma(\boldsymbol{y};\ \boldsymbol{\theta})}{\partial \boldsymbol{h}\partial f_\Delta}\right\} &= \frac{1}{\sigma^2}E\left\{(\mathrm{j}2\pi)\boldsymbol{S}^{\mathrm{H}}\boldsymbol{N}\boldsymbol{G}^{\mathrm{H}}\left(f_\Delta\right)\boldsymbol{y}\right\} \\ &= \frac{1}{\sigma^2}(\mathrm{j}2\pi)\boldsymbol{S}^{\mathrm{H}}\boldsymbol{N}\boldsymbol{G}^{\mathrm{H}}\left(f_\Delta\right)E\left\{\boldsymbol{G}\left(f_\Delta\right)\boldsymbol{S}\boldsymbol{h} + \boldsymbol{n}\right\} \\ &= \frac{1}{\sigma^2}(\mathrm{j}2\pi)\boldsymbol{S}^{\mathrm{H}}\boldsymbol{N}\boldsymbol{S}\boldsymbol{h} \end{aligned} \tag{32}$$

The third and fourth elements of (28) are then derived by determining $\partial\Gamma(\boldsymbol{y};\boldsymbol{\theta})/\partial\boldsymbol{h}^{\mathrm{H}}$

$$\frac{\partial \Gamma(\boldsymbol{y};\ \boldsymbol{\theta})}{\partial \boldsymbol{h}^{\mathrm{H}}} = \frac{1}{\sigma^2}\left\{\boldsymbol{y}^{\mathrm{H}}\boldsymbol{G}(f_\Delta)\boldsymbol{S} + \boldsymbol{h}^{\mathrm{H}}\boldsymbol{S}^{\mathrm{H}}\boldsymbol{S}\right\} \tag{33}$$

The third element of (28) can then be acquired by differentiating (28) with respect to f_Δ and calculating the average, that is

$$\begin{aligned} -E\left\{\frac{\partial^2 \Gamma(\boldsymbol{y};\ \boldsymbol{\theta})}{\partial f_\Delta \partial \boldsymbol{h}^{\mathrm{H}}}\right\} &= \frac{1}{\sigma^2}(-\mathrm{j}2\pi)E\left\{\boldsymbol{y}^{\mathrm{H}}\boldsymbol{N}\boldsymbol{G}\left(f_\Delta\right)\boldsymbol{S}\right\} \\ &= \frac{1}{\sigma^2}(-\mathrm{j}2\pi)\boldsymbol{h}^{\mathrm{H}}\boldsymbol{S}^{\mathrm{H}}\boldsymbol{N}\boldsymbol{S} \end{aligned} \tag{34}$$

Similarly, differentiating (33) with respect to $\boldsymbol{h}$ and calculating the average gives the fourth element of (28)

$$-E\left\{\frac{\partial^2 \Gamma(\boldsymbol{y};\ \boldsymbol{\theta})}{\partial \boldsymbol{h}\partial \boldsymbol{h}^{\mathrm{H}}}\right\} = \frac{1}{\sigma^2}\boldsymbol{S}^{\mathrm{H}}\boldsymbol{S} \tag{35}$$

Finally, the Fisher information matrix $\boldsymbol{J}(\boldsymbol{\theta})$ is obtained by substituting the above four elements in (31), (32), (34) and (35) into (28)

$$\boldsymbol{J}(\boldsymbol{\theta}) = \frac{1}{\sigma^2}\begin{bmatrix} 8\pi^2\boldsymbol{h}^{\mathrm{H}}\boldsymbol{S}^{\mathrm{H}}\boldsymbol{N}^2\boldsymbol{S}\boldsymbol{h} & (-\mathrm{j}2\pi)\boldsymbol{h}^{\mathrm{H}}\boldsymbol{S}^{\mathrm{H}}\boldsymbol{N}\boldsymbol{S} \\ (\mathrm{j}2\pi)\boldsymbol{S}^{\mathrm{H}}\boldsymbol{N}\boldsymbol{S}\boldsymbol{h} & \boldsymbol{S}^{\mathrm{H}}\boldsymbol{S} \end{bmatrix} \tag{36}$$

The CRLB of $\{f_\Delta, \boldsymbol{h}\}$ is also obtained by inversion of the Fisher information [27]

$$\begin{aligned} &\mathrm{var}(f_\Delta) \geq \left[\boldsymbol{J}^{-1}(\boldsymbol{\theta})\right]_{11} \\ &\mathrm{var}(h(l)) \geq \left[\boldsymbol{J}^{-1}(\boldsymbol{\theta})\right]_{(l+1)(l+1)}, \quad l = 0,\ 1,\ \ldots,\ L-1 \end{aligned} \tag{37}$$

It is noteworthy that the inversion of $\boldsymbol{J}(\boldsymbol{\theta})$ can be derived to acquire the closed-form equation via the property of the Woodbury matrix identity [28]. That is, based on the orthonormal property of Zadoff–Chu sequences, that is, $\boldsymbol{S}^{\mathrm{H}}\boldsymbol{S} = \boldsymbol{I}_{L\times L}$ in (3), the Fisher information matrix $\boldsymbol{J}(\boldsymbol{\theta})$ in (36) can be rewritten as

$$\boldsymbol{J}(\boldsymbol{\theta}) = \frac{1}{\sigma^2}\begin{bmatrix} \alpha & \boldsymbol{u}^{\mathrm{H}} \\ \boldsymbol{u} & \boldsymbol{I} \end{bmatrix} \tag{38}$$

where $\alpha = 8\pi^2\boldsymbol{h}^{\mathrm{H}}\boldsymbol{S}^{\mathrm{H}}\boldsymbol{N}^2\boldsymbol{S}\boldsymbol{h}$ and $\boldsymbol{u} = (\mathrm{j}2\pi)\boldsymbol{S}^{\mathrm{H}}\boldsymbol{N}\boldsymbol{S}\boldsymbol{h}$. The Woodbury matrix identity property can be used to derive $\boldsymbol{J}^{-1}(\boldsymbol{\theta})$ as follows

$$\boldsymbol{J}^{-1}(\boldsymbol{\theta}) = \sigma^2\begin{bmatrix} \beta & -\beta\boldsymbol{u}^{\mathrm{H}} \\ -\beta\boldsymbol{u} & \boldsymbol{I} + \beta\boldsymbol{u}\boldsymbol{u}^{\mathrm{H}} \end{bmatrix} \tag{39}$$

where $\beta = (\alpha - \boldsymbol{u}^{\mathrm{H}}\boldsymbol{u})^{-1}$. Therefore the CRLB of $\{f_\Delta, \boldsymbol{h}\}$, that is, the diagonal element of $\boldsymbol{J}^{-1}(\boldsymbol{\theta})$ in (37), can be directly determined by (39) without the matrix inversion.

Finally, the CRLB of $\{f_\Delta, \boldsymbol{h}\}$ is used as a benchmark in performance comparisons of the proposed CFO and CIR estimation algorithms. The results of the performance comparisons are given in the following section.

5 Simulation results

Simulation results are demonstrated to reveal the merits of the proposed iterative JML-CMV CFO and CIR estimation algorithms for OFDMA downlink systems in the cell-edge scenario. The channel profile assumed in all simulations was an $L = 4$ independent frequency selective Rayleigh fading channel with four equal-power paths, and time delays are chosen from $[0,\ 3T_{\mathrm{s}}]$ (T_{s} being the sampling time), which is smaller than the CP length $N_g = 16$. A quasi-static fading channel was assumed to be constant during each packet and assumed to be independent between packets. The fading gains were the independent and identically distributed (i.i.d.) complex Gaussian random variables with zero mean and unity variance. The number of subcarriers used for preamble symbol sequence was chosen to be $N = 64$. All preamble sequences were generated by Zadoff–Chu sequences [23], which were used as the training codes. Also, the assumed range of frequency offsets between the user and all cells was $f_\Delta = [-0.5,\ 0.5]$. For use as a performance index, the average MSEs of CFO and CIR are defined as

$$\mathrm{MSE\_CFO} = \frac{1}{3M}\sum_{i=0}^{2}\sum_{m=1}^{M}\left|\hat{f}_{\Delta,m}^{(i)} - f_{\Delta,m}^{(i)}\right|^2 \tag{40}$$

$$\mathrm{MSE\_CIR} = \frac{1}{3ML}\sum_{i=0}^{2}\sum_{l=0}^{L-1}\sum_{m=1}^{M}\left|\hat{h}_m^{(i)}(l) - h_m^{(i)}(l)\right|^2 \tag{41}$$

and the average output preamble SINR (output PSINR) is

doi: 10.1049/iet-com.2013.0092

defined as

$$\text{output PSINR} = \frac{1}{3}\sum_{i=0}^{2}\text{OPSINR}_i \tag{42}$$

(see (43))

where m is the mth Monte Carlo trial. The $\{\hat{f}_{\Delta,m}^{(i)}, \hat{h}_m^{(i)}(l)\}$ and $\{f_{\Delta,m}^{(i)}, h_m^{(i)}(l)\}$ are the mth estimated and true CFO and CIR parameters, respectively. Notably, the average MSE and output PSINR performances are provided for use in judging the estimated performance of the boundary cell user. Next, $M = 10\,000$ trials were executed to obtain each outputs MSE and PSINR values. A different set of CFOs and CIRs were used in each trial. The input SNR was also defined as the SNR_i dB $= 10\log_{10}\left(\sigma_i^2/\sigma_n^2\right)$ of the ith desired cell, and the jth other-cell-to-desired-cell signal ratio (OSR) was defined as OSR dB $= 10\log_{10}(\sigma_j^2/\sigma_i^2)$, where σ_i^2 and σ_j^2 are the signal power of the ith and jth cells, respectively. Next, the worst case of the same received signal power from different cells, that is, $\sigma_i^2 = \sigma_j^2$, $i \neq j$, was considered. Performance was compared in terms of the results obtained by the JML CFO and CIR estimators proposed by Hwang *et al.* [17], the ideal CRLB in Section 4, the ideal output PSINR and the proposed iterative estimator in Section 3. The ideal output PSINR result was calculated by substituting the ideal weight vectors in (13) and (22) with true CIR and CFO into the output PSINR formula in (43) to obtain an indicator of ideal performance. Finally, the following 'standard' parameters are used throughout this section unless noted otherwise: $\text{SNR}_i = 15$ dB, OSR = 0 dB, $N = 64$, $N_g = 16$, $L = 4$, $M = 10\,000$ and $f_\Delta = [-0.5, 0.5]$.

In the first set of simulations, the MSE_CFO performance is evaluated as a function of input SNR for the ideal CRLB and the iterative estimator of the proposed receiver. Fig. 5 shows the comparison results, which confirm that the proposed estimator outperforms the conventional JML-CFO estimator developed by Hwang and successively approaches the ideal CRLB CFO performance. Degradation is limited to approximately 1 dB in six iterations. The relatively poor performances of the Hwang JML-CFO estimator and the first iteration of the proposed JML-CFO estimator result from ICI interference, that is, the adjacent-cell preamble sequence with CFO effect. Besides, the proposed JML-CFO estimator also outperforms the popular cross-correlation-based method first reported in (4). Notably, the performance of the cross-correlation-based method is severely degraded by strong cell-edge interference. Next, the results of six iterations in Fig. 5 are shown that the performance of the proposed JML-CFO estimator with interference cancellation almost equals the desired single-cell performance, which confirms the assertion made in Section 4.

In the second set of simulations, the MSE_CIR performance is evaluated as a function of input SNR. Fig. 6 shows the comparison results, which confirm that the proposed CMV-CIR estimator with iterative cancellation outperforms the conventional JML-CIR estimator developed by Hwang and successively improves with each iteration until it approaches the ideal CRLB CIR performance with a degradation limited to approximately 1.5 dB in six iterations. Besides, as the number of iterations increases, the proposed CMV_CIR estimator also outperforms the linear LS channel estimator in (7). The relatively poor performance of the LS estimator results from its projection matrix design, which does not consider the effects of CFO estimation error and noise. Notably, comparison of Figs. 5 and 6 further shows that degradation is higher in the CMV-CIR estimator than in the JML-CFO estimator since the CIR estimation is degraded by a mismatched CFO-shifted preamble vector (13) caused by the CFO

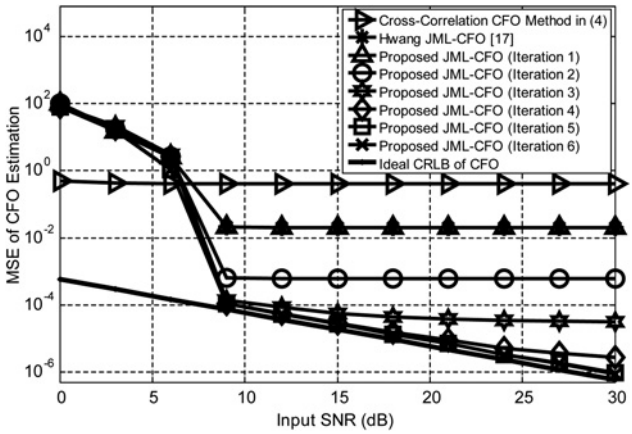

Fig. 5 *MSE performance of the proposed JML-CFO estimator for OFDMA downlink systems with three cell interferences over multipath fading channels*

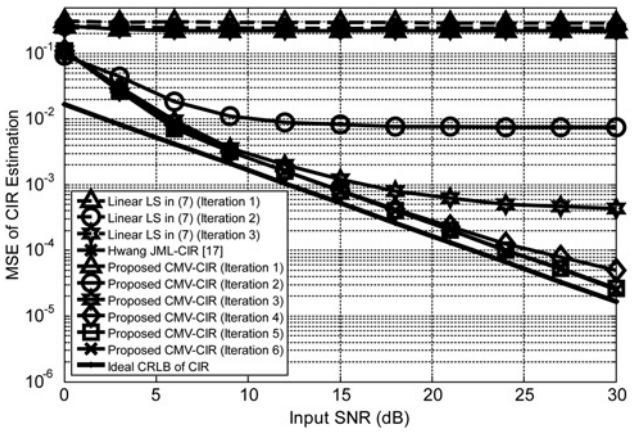

Fig. 6 *MSE performance of the proposed CMV-CIR estimator for OFDMA downlink systems with three cell interferences over multipath fading channels*

$$\text{OPSINR}_i = 10\log_{10}\frac{\dfrac{1}{ML}\displaystyle\sum_{l=0}^{L-1}\sum_{m=1}^{M}\left|\boldsymbol{w}_{l,m}^{(i)\text{H}}\mathbf{G}(f_{\Delta,m}^{(i)})\boldsymbol{s}_l^{(i)}h_m^{(i)}(l)\right|^2}{\dfrac{1}{2ML}\displaystyle\sum_{\substack{j=0\\(j\neq i)}}^{2}\sum_{l=0}^{L-1}\sum_{m=1}^{M}\left|\boldsymbol{w}_{l,m}^{(i)\text{H}}\mathbf{G}\left(f_{\Delta,m}^{(j)}\right)\boldsymbol{s}_l^{(j)}h_m^{(j)}(l)\right|^2 + \dfrac{1}{L}\displaystyle\sum_{l=0}^{L-1}\sigma_n^2\boldsymbol{w}_{l,m}^{(i)\text{H}}\boldsymbol{w}_{l,m}^{(i)}} \tag{43}$$

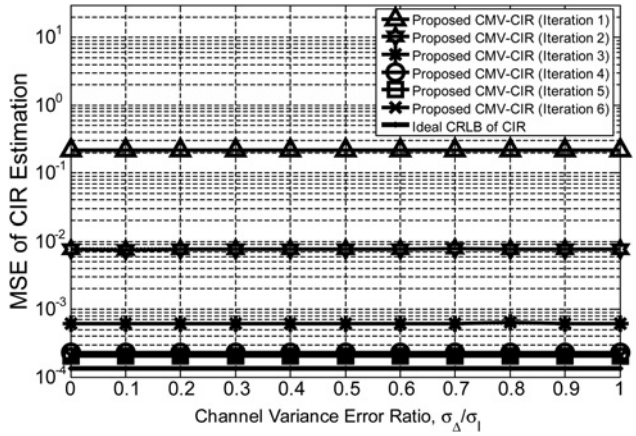

Fig. 7 *MSE performance of the proposed CMV-CIR estimator against relative channel variance error over multipath fading channels*

estimation error. Nevertheless, the results in Fig. 6 confirm that the proposed iterative estimator effectively suppresses adjacent-cell interference.

In the third set of simulations, the robustness of the proposed estimator against the correlation matrix $\boldsymbol{R}_{yy}$ errors is demonstrated. In this case, $\boldsymbol{R}_{yy}$ in (17) involves the estimated CFO error via JML-CFO estimator. Moreover, we consider the effect of channel variance error $\tilde{\sigma}_l^{(i)}$, that is, $\tilde{\sigma}_l^{(i)} = \sigma_l^{(i)} + \Delta\sigma_l^{(i)}$ with $\Delta\sigma_l^{(i)}$ being the i.i.d. Gaussian random variable with variance σ_Δ^2. Fig. 7 shows the MSE_CIR performance against σ_Δ/σ_l with the equal-power channel profile for different paths. The comparison results confirm that the proposed CMV estimator provides highly reliable channel estimation for the correlation matrix $\boldsymbol{R}_{yy}$ error with the estimated CFO and channel variance errors.

In the fourth set of simulations, the robustness of the proposed iterative estimator against severe CFOs is demonstrated. Here, the normalised CFO range as formulated in (3) was $f_\Delta = [-0.5, 0.5] + f_{\text{int}}$, where f_{int} is an integer CFO within a range of [0, 8]. The simulation was simplified by setting $f_{\text{int}} = [0, 1, 2, 4, 8]$. Fig. 8 shows the MSE_CFO and MSE_CIR results after six simulations. The simulation results confirm the reliable performance of the proposed iterative estimator up to a CFO with $f_\Delta = [-0.5, 8.5]$ in the JML-CFO and CMV-CIR estimators. Notably, the CFO range was simulated under realistic conditions such as those that occur in digital video broadcasting terrestrial (DVB-T), LTE and WiMAX applications.

In the fifth set of simulations, the output PSINR performance of the proposed iterative estimator is evaluated and compared with the ideal output PSINR performance with perfect CFO and CIR. Fig. 9 plots the resulting output PSINR curves as a function of input SNR. The comparison results confirm that the proposed estimator successively approaches the ideal output PSINR performance with degradation limited to approximately 1 dB in six iterations when input SNR = 30 dB. Notably, good desired-cell signal reception and effective suppression of adjacent-cell interference by the iterative receiver provides sufficiently accurate CFO and CIR estimates to ensure a high output PSINR.

In the sixth set of simulations, to demonstrate the effectiveness of the proposed estimator for the large channel length, that is, $L = 10$, with the exponential-power delay profile, the output PSINR performance is evaluated as a function of input SNR. In this simulation, CFO and CIR parameters were estimated by using the Zadoff–Chu sequences typically used in LTE systems, that is, 25, 29

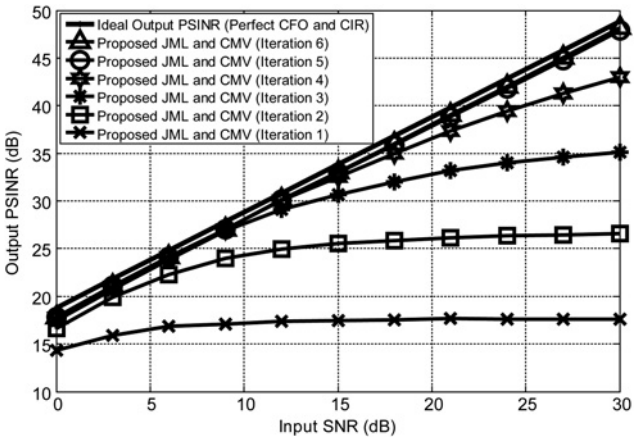

Fig. 9 *Output PSINR performance of the proposed iterative JML-CFO and CMV-CIR estimators for OFDMA downlink systems with different input SNR over multipath fading channels*

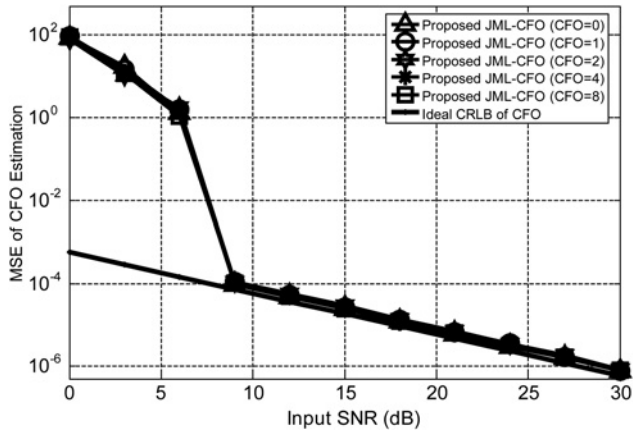

Fig. 8 *MSE performance of the proposed JML-CFO estimator with different CFOs for OFDMA downlink system over multipath fading channels*

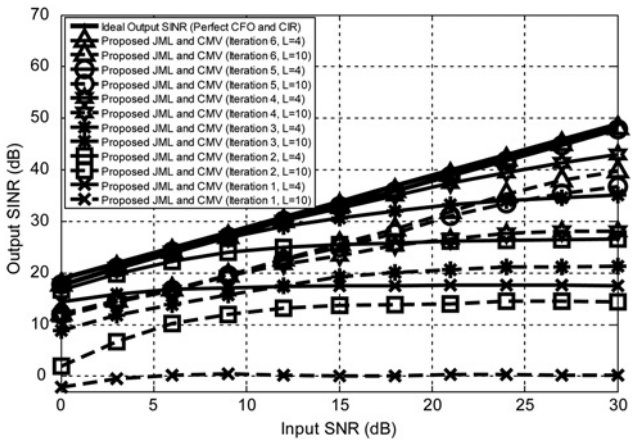

Fig. 10 *Output PSINR performance of the proposed iterative JML-CFO and CMV-CIR estimators over different channel length with different power profiles*

doi: 10.1049/iet-com.2013.0092

and 34. Fig. 10 shows the output PSINR performance results obtained by the proposed estimator for the $L = 4$ equal-power and $L = 10$ exponential-power multipath channel profiles. Notably, the performance of the proposed estimator with the LTE-based Zadoff–Chu sequences improves as the number of iteration increases. The estimation results confirm the effectiveness of the proposed estimator for use in the large channel length scenario. However, as Fig. 10 shows, the performance degradation of the proposed estimator is larger in the $L = 10$ large channel profile compared with the $L = 4$ small size channel environment. Notably, the degraded system performance results from the increased channel size in the projection matrix $\boldsymbol{P}_{\bar{\boldsymbol{S}}}$ given in (10) with the larger column span of $\bar{\boldsymbol{S}}$, which induces a noise enhancement problem.

In the seventh set of simulations, the output PSINR performance of the proposed iterative estimator for the desired cell is evaluated under the adjacent cell with different interference powers, that is, OSR values. That is, the blocking and shadowing effects induce the signal attenuation or loss between the desired cell and user in this case. Fig. 11 shows the output PSINR curves, which confirm that the proposed iterative estimator achieves excellent resistance by effectively using the degree of freedom of the preamble sequence to cancel strong adjacent-cell interference.

Finally, in the eighth set of simulations, the effectiveness of the iterative estimator for different degrees of freedom offered by the preamble sequence is demonstrated. Here, the two scenarios with different preamble sequence sizes explore the output PSINR performance. First, for the practical OFDMA downlink, the number of available subcarriers is less than $N = 64$ because of the edge and DC subcarriers being used for band protections. Therefore, in this case, we simulate the output PSINR performance as a function of varying the useful subcarrier sizes $3 \times M$ in (2). As shown in Fig. 12, the proposed iterative estimator successively approaches the ideal output PSINR performance with a slight degradation of about 2 dB at the sixth iteration from the useful subcarriers being 63 down to 42. It is because of the short-length time-domain Zadoff–Chu sequence with small degree of freedom and the degradation of the autocorrelation and cross-correlation properties. Next, for another scenario, the total length $N = 64$ of the preamble sequence in (1) are replaced by Zadoff–Chu sequence codes

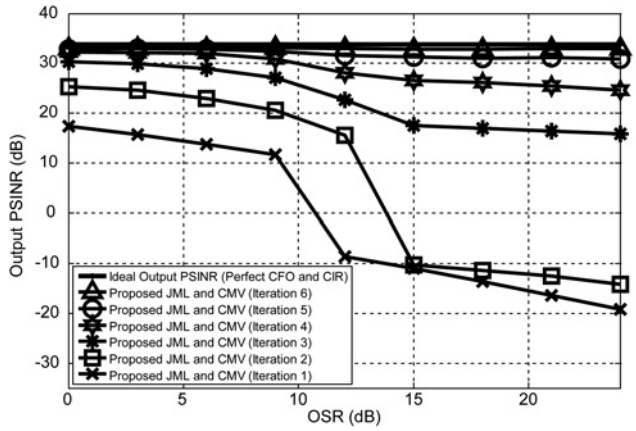

Fig. 11 *Output PSINR performance of the proposed iterative JML-CFO and CMV-CIR estimators for OFDMA downlink systems with different OSR over multipath fading channels*

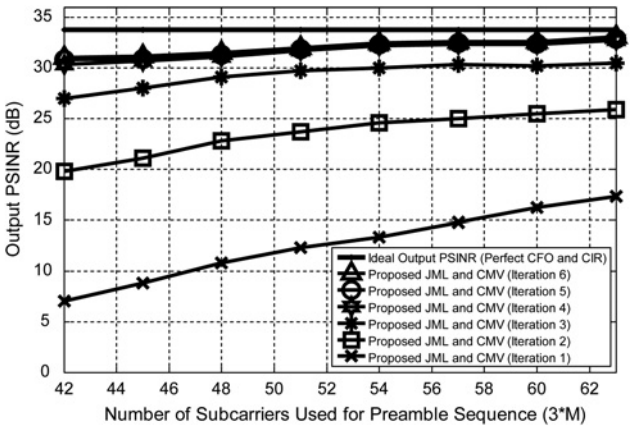

Fig. 12 *Output PSINR performance of the proposed iterative JML-CFO and CMV-CIR estimators for OFDMA downlink systems with different available subcarriers used for preamble sequence over multipath fading channels*

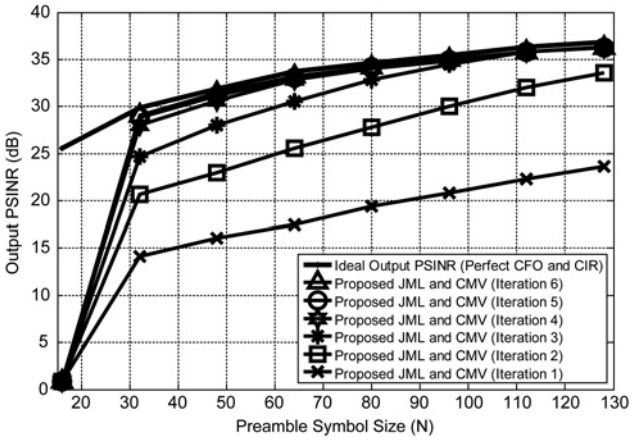

Fig. 13 *Output PSINR performance of the proposed iterative JML-CFO and CMV-CIR estimators for OFDMA downlink systems with different preamble symbol size over multipath fading channels*

of varying lengths. Fig. 12 shows the output PSINR performance as a function of varying sizes of N. The performance comparison results again confirm the reliability of the proposed iterative estimator from $N = 128$ down to 32. Degradation is limited to approximately 1 dB in output PSINR. Notably, Fig. 13 shows that, at $N = 16$, the response of the proposed estimator with a short preamble sequence is inadequate for suppressing the adjacent-cell interferences. Therefore output PSINR substantially decreases. However, the simulation results confirm that the proposed iterative estimator is able to offer the robust output PSINR performance with a moderate preamble symbol size in the presence of severe adjacent-cell interference.

6 Conclusions

In this study, the efficient JML and CMV algorithms with iterative interference cancellation were developed to estimate CFO and CIR parameters for cell-edge user communication. The JML method reduces the complexity of CFO estimations by applying polynomial approach and iterative zoom-FFT techniques. The CMV algorithm also

enhances CIR estimation accuracy by suppressing cell interference. The simulation results confirm that the proposed algorithm iteratively provides CFO and CIR estimations with accuracies approaching those of the ideal CRLB and output PSINR under severe adjacent-cell interference conditions.

7 Acknowledgments

This work was sponsored by the National Science Council, R. O.C., under the contract nos. NSC 102–2220-E-155–006 and NSC 102–2218-E-155–001. The authors express the deepest gratitude to Professor Jeng-Kuang Hwang for his kind help and enthusiastic guidance. The authors also thank the editor and anonymous reviewers for their helpful comments and suggestions in improving the quality of this article.

8 References

1 IEEE 802.16e standard: 'Air interface for fixed and mobile broadband wireless access systems', 2005
2 3GPP: '3rd generation partnership project; technical specification group radio access network; physical layer aspects for evolved UTRAN', TR v7.1.0
3 Chiueh, T.D., Tsai, P.U.: 'OFDM baseband receiver design for wireless communications' (John Wiley & Sons, 2007)
4 Han, D.S., Seo, J.H., Kim, J.J.: 'Fast carrier frequency offset compensation in OFDM systems', *IEEE Trans. Consum. Electron.*, 2001, **47**, (3), pp. 364–369
5 Kim, Y.H., Song, I., Yoon, S., Park, S.R.: 'An efficient frequency offset estimator for OFDM systems and its performance characteristics', *IEEE Trans. Veh. Technol.*, 2001, **50**, (5), pp. 1307–1312
6 Deneire, L., Vandenameele, P.L., Perre, V.D., Guselinckx, B., Engels, M.: 'A low-complexity ML channel estimator for OFDM', *IEEE Trans. Commun.*, 2003, **51**, (2), pp. 135–140
7 Morelli, M., Mengali, U.: 'A comparison of pilot-aided channel estimation methods for OFDM systems', *IEEE Trans. Signal Process.*, 2001, **49**, (12), pp. 3065–3073
8 Weng, L., Au, E.K.S.P., Chan, W.C., *et al.*: 'Effect of carrier frequency offset on channel estimation for SISO/MIMO-OFDM systems', *IEEE Trans. Wirel. Commun.*, 2007, **6**, (5), pp. 1854–1863
9 Salari, S., Ardebilipour, M., Ahmadian, M.: 'Joint carrier frequency offset and channel estimation for MIMO-OFDM transmission', *Wirel. Pers. Commun.*, 2008, **47**, (2), pp. 303–314
10 Lee, J.H., Han, J.C., Kim, S.C.: 'Joint carrier frequency synchronization and channel estimation for OFDM systems via the EM algorithm', *IEEE Trans. Veh. Technol.*, 2006, **55**, (1), pp. 167–172
11 Moon, T.: 'The expectation-maximization algorithm', *IEEE Signal Process. Mag.*, 1996, **13**, (6), pp. 47–60
12 Salari, S.: 'Iterative receiver design with joint carrier frequency offset and channel estimation for LDPC-coded MIMO-OFDM Systems', *Wirel. Pers. Commun.*, 2012, **62**, (1), pp. 127–138
13 Pun, M.O., Morelli, M., Kuo, C.C.J.: 'Maximum likelihood synchronization and channel estimation for OFDMA uplink transmissions', *IEEE Trans. Commun.*, 2006, **54**, (4), pp. 726–736
14 Ziskind, I., Wax, M.: 'Maximum likelihood localization of multiple sources by alternating projection', *IEEE Trans. Acoust. Speech Signal Process.*, 1998, **36**, (10), pp. 1553–1560
15 Chen, J., Wu, Y.C., Ng, T.S.: 'Optimal joint CFO and channel estimation in quasi-synchronized OFDM systems', *IEEE Globecom*, 2007, pp. 2816–2820
16 Morelli, M., Mengali, U.: 'Carrier-frequency estimation for transmissions over selective channels', *IEEE Trans. Commun.*, 2000, **48**, (9), pp. 1580–1589
17 Hwang, J.K., Chung, R.L., Liao, T.H.: 'Highly efficient algorithm for joint ML estimation of carrier frequency offset and channel for OFDM transmissions'. IEEE Int. Symp. Consumer Electronics, 2009, pp. 351–354
18 Lee, D., Seo, H., Clerckx, B., *et al.*: 'Coordinated multipoint transmission and reception in LTE-advanced: deployment scenarios and operational challenges', *IEEE Commun. Mag.*, 2012, **50**, (2), pp. 148–155
19 Zarifi, K., Gershman, A.B.: 'High SNR performance analysis of blind minimum output energy receivers for large DS-CDMA systems', *IEEE Trans. Signal Process.*, 2008, **56**, (7), pp. 3248–3260
20 Van Veen, B.D., Buckley, K.M.: 'Beamforming: a versatile approach to spatial filtering', *IEEE ASSP Mag.*, 1998, **5**, (2), pp. 4–24
21 Fu, X., Minn, H., Cantrell, C.D.: 'Two novel iterative joint frequency-offset and channel estimation methods for OFDMA uplink', *IEEE Trans. Commun.*, 2008, **56**, (3), pp. 474–484
22 Zhang, X.P., Ryu, H.G.: 'Suppression of ICI and MAI in SC-FDMA communication system with carrier frequency offsets', *IEEE Trans. Consum. Electron.*, 2010, **56**, (2), pp. 359–365
23 Li, C.P., Huang, W.C.: 'A constructive representation for the Fourier dual of the Zadoff-Chu sequences', *IEEE Trans. Inf. Theory*, 2007, **53**, (11), pp. 4221–4224
24 Moose, P.H.: 'A technique for orthogonal frequency division multiplexing frequency offset correction', *IEEE Trans. Commun.*, 1994, **42**, (10), pp. 2908–2914
25 Schmidl, T.M., Cox, D.C.: 'Robust frequency and timing synchronization for OFDM', *IEEE Trans. Commun.*, 1997, **45**, (12), pp. 1613–1621
26 Hoyer, E., Stork, R.: 'The zoom FFT using complex modulation', *IEEE ICASSP*, 1977, **2**, pp. 78–81
27 Kay, S.M.: 'Fundamentals of statistical signal processing: estimation theory' (Prentice-Hall, Englewood Cliffs, NJ, 1993)
28 Press, W.H., Teukolsky, S.A., Vetterling, W.T., Flannery, B.P.: 'Numerical recipes 3rd edition: the art of scientific computing' (Cambridge University Press, New York, 2007), Chap. 2.7.3

doi: 10.1049/iet-com.2013.0092